Meccanica (2016) 51:2847–2859
DOI 10.1007/s11012-016-0510-3

Damage identification in a parabolic arch by means of natural frequencies, modal shapes and curvatures

Danilo Capecchi · Jacopo Ciambella · Annamaria Pau · Fabrizio Vestroni

Received: 10 March 2016 / Accepted: 1 August 2016 / Published online: 10 August 2016

Abstract This paper investigates damage identification techniques based on the difference of modal frequencies, shapes and curvatures in the damaged and undamaged states of the structure. The sensitivity of the identification algorithm with respect to damage parameters is discussed and the minimum number of measured quantities to identify the damage is assessed. It is shown that modal curvatures can be effectively used to pre-localise the damage and to add a penalty term in the objective function which weighs the difference between natural frequencies and modal displacements. Such a term improves the local convexity of the objective function and enhances the convergence rate of the minimization algorithm. The procedure is validated against the results of the experiments on a parabolic arch carried out by the authors. The advantages of such an approach compared to techniques solely based on frequencies are that the ill-conditioning of the inverse problem is reduced and a more accurate estimate of the damage parameters is achieved.

Keywords Damage detection · Damage localization · Inverse problems · Arch dynamics · Modal quantities

D. Capecchi · A. Pau (✉)
Department of Structural and Geotechnical Engineering, SAPIENZA University of Rome, Via Gramsci 53, 00197 Rome, Italy
e-mail: danilo.capecchi@uniroma1.it

A. Pau
e-mail: annamaria.pau@uniroma1.it

J. Ciambella · F. Vestroni
Department of Structural and Geotechnical Engineering, SAPIENZA University of Rome, Via Eudossiana 18, 00184 Rome, Italy
e-mail: jacopo.ciambella@uniroma1.it

F. Vestroni
e-mail: vestroni@uniroma1.it

1 Introduction

Over the last few decades, many authors have investigated structural health monitoring techniques based on measurement of the modal response (see, for instance [1], for a comprehensive review). This increasing interest has been backed up by the fast technological advances, which have made available a number of low-cost and reliable sensors suitable to monitor the state of large civil constructions including buildings, bridges and aqueducts [2–4]. Owing to the easiness and robustness of measuring frequencies compared to other modal quantities, the use of their changes has been one of the first approaches used in damage detection [5–9]. However, frequencies suffer the well-known limitation of having a low sensitivity with respect to local variations of the mechanical characteristics [10] which could lead to significant errors in the identified parameters. Moreover, damage

detection techniques based on eigenfrequencies lead to a class of inverse problems which are often ill-conditioned and sometimes undetermined. Suitable solutions to inverse problems for frequency-based damage detection mostly dealt with straight [11–13] rather than curved beams [14, 15].

To overcome these limitations, many researchers have focused their efforts on measuring and using the changes on modal shapes and curvatures [16, 17, and references therein]. The use of modal curvatures in damage detection procedures dates back to the seminal work of Pandey et al. [18]. Since then, many authors have used modal curvatures for the problem of damage localization and assessment in beams [16, 19–21] and beam-like structures [22, 23]. From the theoretical point of view, modal curvatures are effective observable quantities as, for narrow damages, they are localized in the region of the damage. Broader damages cause the modal curvature difference to have several peaks outside the damaged region that could result in a false damage localization [17]. Effective damage identification has been obtained by various filtering techniques including spline interpolation [24], wavelet transforms [25] or modified Laplace operator [26]. However, in those papers, a high number of measurement points is used to obtain reliable values of modal curvatures.

In this work, we propose an updated identification procedure following the approach in [6] and [27]: the identification of the damage is obtained through the minimization of an objective function measuring the differences between numerical and experimental natural frequencies as well as modal shapes and curvatures in the damaged and undamaged states. Despite being adopted in many identification techniques, the use of modal curvatures could be problematic as their evaluation requires a large number of measurement points. However, even with a limited number of points, their changes can give an important contribution in damage localization when used with other modal quantities and help in achieving a more robust estimate of the damage parameters.

This identification technique is illustrated with reference to parabolic arches, which have received far less attention than beams. The arch is studied by using a finite element model in both the direct and the inverse problems. The sensitivity of the modal properties with respect to the damage parameters are assessed and it is shown that more pieces of information are necessary to uniquely determine the position and the intensity of the damage compared to straight beams.

The paper is organized as follows: in Sect. 2 a model for the cracked arch is described and used in Sect. 3 to assess the effects of damage on the modal response. In Sect. 4 the inverse problem is studied and the conditioning of the problem is discussed. In Sect. 5, the proposed technique is validated against the results of the experiments carried out by the authors on a steel parabolic arch. Finally, conclusions are drawn in Sect. 6.

2 Description of the cracked arch under investigation

A double-hinge parabolic plane arch with the following centerline equation is considered:

$$y(x) = 4f\frac{x}{L}\left(1-\frac{x}{L}\right) \tag{1}$$

where $f = 200$ mm is the mid-span height and $L = 1000$ mm is its projection onto a horizontal axis, as shown in Fig. 1. The size of the rectangular cross section and the values of Young's modulus E, Poisson's ratio v and mass density m are also reported in Fig. 1.

It is assumed that the arch has a localized notch that reduces the height of the cross section from h^U to h^D and that the notch width is small enough not to affect the total structural mass. At a given normalised abscissa $s = x/L$, such a damage determines a reduction in the flexural and axial stiffness, the latter of which is ignored in the damage model for its negligible influence on the modal characteristics of non-shallow slender arches, such as the one considered here (see [28]). Moreover, a refined model of damage accounting for changes in axial stiffness would be necessary only for damages smaller than the ones considered here [27]. To model the effect of the local damage, a rotational spring is introduced and its stiffness is calculated as shortly summarized in the following. The notch causes a perturbation of the stress state in a zone whose length L^D is greater than the effective width of the notch itself. The relative rotation ϕ^D between the cross-section sections delimiting the damaged zone can be written as $\phi^D = \phi^U + \Delta\phi$, where ϕ^U is the rotation between the two limit sections in the

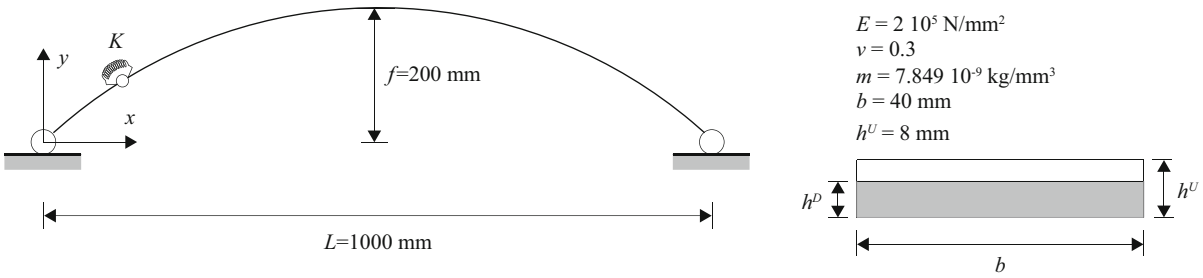

Fig. 1 Geometric and mechanic properties of the arch under investigation. The crack is modeled as a rotational spring

undamaged case and $\Delta\phi$ is the increase in rotation due to damage. For a small L^D, $\Delta\phi$ can be expressed as

$$\Delta\phi = M\frac{L^D}{EI^U}\frac{\beta}{1-\beta} \tag{2}$$

where $\beta = (EI^U - EI^D)/EI^U$, with EI^U and EI^D respectively the flexural rigidities of the undamaged and damaged cross sections; $L^D = h/2$ is assumed here. This result is obtained by requiring that the deformability of a beam with a distributed exponential decay equals the deformability of a beam with a step change of stiffness with length L^D. In the end, the equivalent stiffness of the localized spring is expressed as $K = M/\Delta\phi$, with its nondimensional value $k = K/(EI^U/L_a)$ expressed by

$$k = \frac{2L_a}{h^U}\frac{1-\beta}{\beta} \tag{3}$$

where L_a is the total length of the parabolic arch measured along its axis. Therefore, the concentrated damage will be characterized in terms of position s and intensity k.

3 Sensitivity of the modal quantities

Owing to the arch slenderness and the negligible shear deformation, one thousand Euler–Bernoulli beam two-node elements were used in the simulation. Such a high number of elements provides stable frequencies, varying less than 1 ‰ by increasing further the number of nodes, and allows a very accurate description of the curvature. Damage has been modelled by releasing the relative rotation of two adjacent nodes and connecting them with a rotational spring element. The model also includes lumped mass elements that represent the added masses of the accelerometers. The system does not have close frequencies (Fig. 2) and the prevailing displacement component of the first low modes is orthogonal to the axis of the arch. In contrast to the flexural behaviour of straight beams, the arch has skew–symmetric odd modes and symmetric even modes. Figure 3 shows the relative variation of frequency between the undamaged and damaged states in terms of damage normalised location s and intensity k for an arch and a straight beam with the same cross-section properties and length L. The structure being symmetric, the changes in frequencies at two symmetric locations are the same and only half of the axis is shown. It is seen that for each frequency, differences reach their maximum when the damage is located where the curvature reaches its higher values (see Fig. 2), while is equal to zero when the damage is located at a node [14]. This circumstance can be used to investigate the weakness of inverse procedures for damage characterization solely based on frequency variations. If ω_i represents the i-th frequency of the damaged arch for given values of k and s, we can represent the values of the equivalent stiffness $k_i(s)$ that for every position s provides the same ω_i. This function is shown in Fig. 4 for an arch and a beam.

The curves $k_i(s)$ would intersect at the abscissa where damage is actually located, providing the solution to the inverse problem. In the case of the simply supported beam (Fig. 4b), the curves corresponding to the first and the second frequencies (with label 1 and 2 in the figure) intersect at one point which corresponds to the solution of the inverse problem with only two frequencies. On the contrary, the same pair of curves for the arch has more than one intersection, making the solution of the inverse

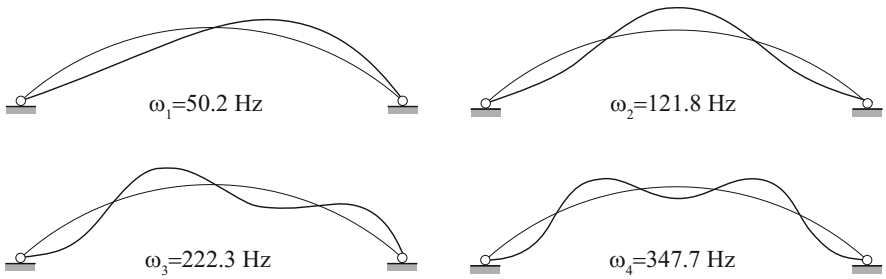

Fig. 2 The first four mode shapes and corresponding frequencies of the undamaged arch obtained by FE analsys

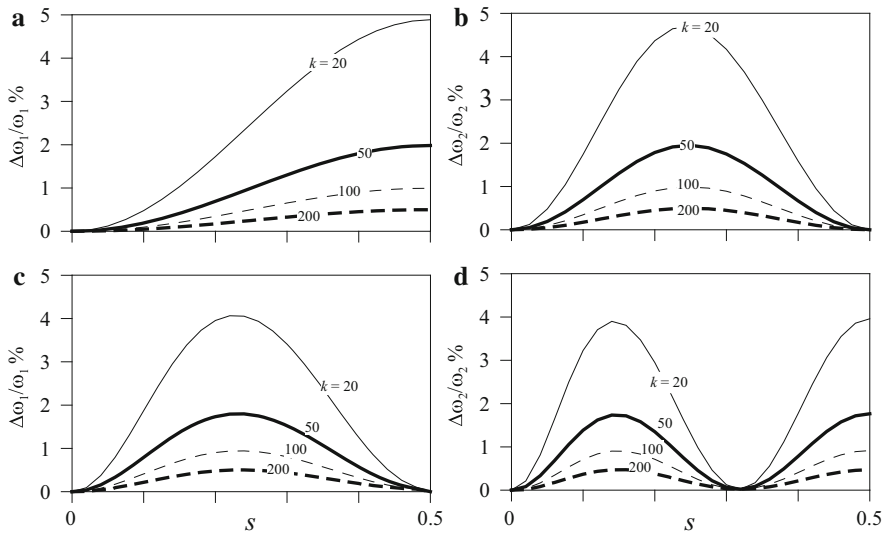

Fig. 3 Relative frequency variations as a function of the damage parameters k and s for the first two modes of a beam (**a**, **b**) and an arch (**c**, **d**) with the same cross section properties and length. Due to the symmetry of the results only half span is reported

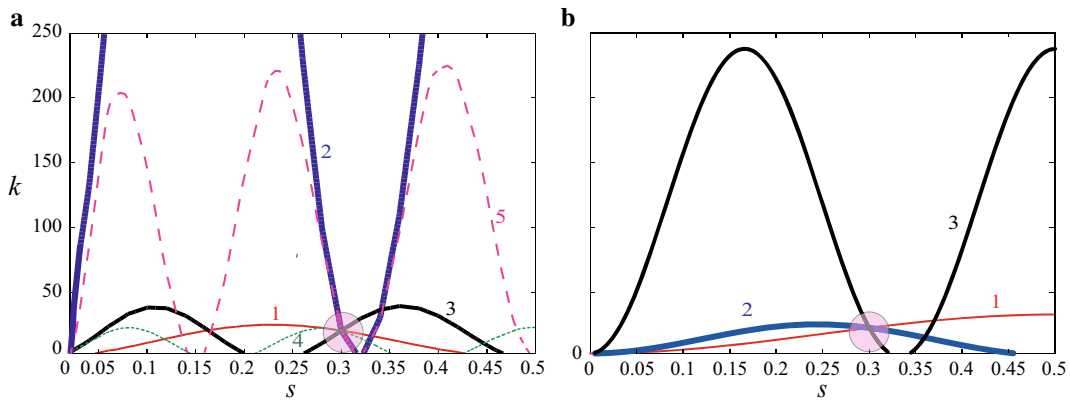

Fig. 4 Curves $k_i(s)$ for the first five modes of the arch (**a**) and three modes of the beam (**b**); $s = 0.30$, $k = 20$. Due to the symmetry of the problem only half structure is shown

problem with only two frequencies undetermined. As such, at least three frequencies are needed to uniquely determine the two damage parameters of the arch. Moreover, the presence of close intersections in Fig. 4a warns against possible errors arising in the presence of experimental noise which suggests that a higher number of modal quantities should be used to achieve a more robust evaluation of damage.

In this respect, Fig. 5 shows the changes in the displacement normal components of the first and second modes, normalized with respect to the modal mass, for two damage locations. For increasing damage intensity, the differences increase at the damage location; however, the same figure shows that there are multiple peaks outside the damaged region that could not give a clear indication of damage position. A more accurate localisation can be achieved by using the modal curvature difference. Figure 6 shows the modal curvatures variations, where a sharp peak in the modal curvatures differences is located in

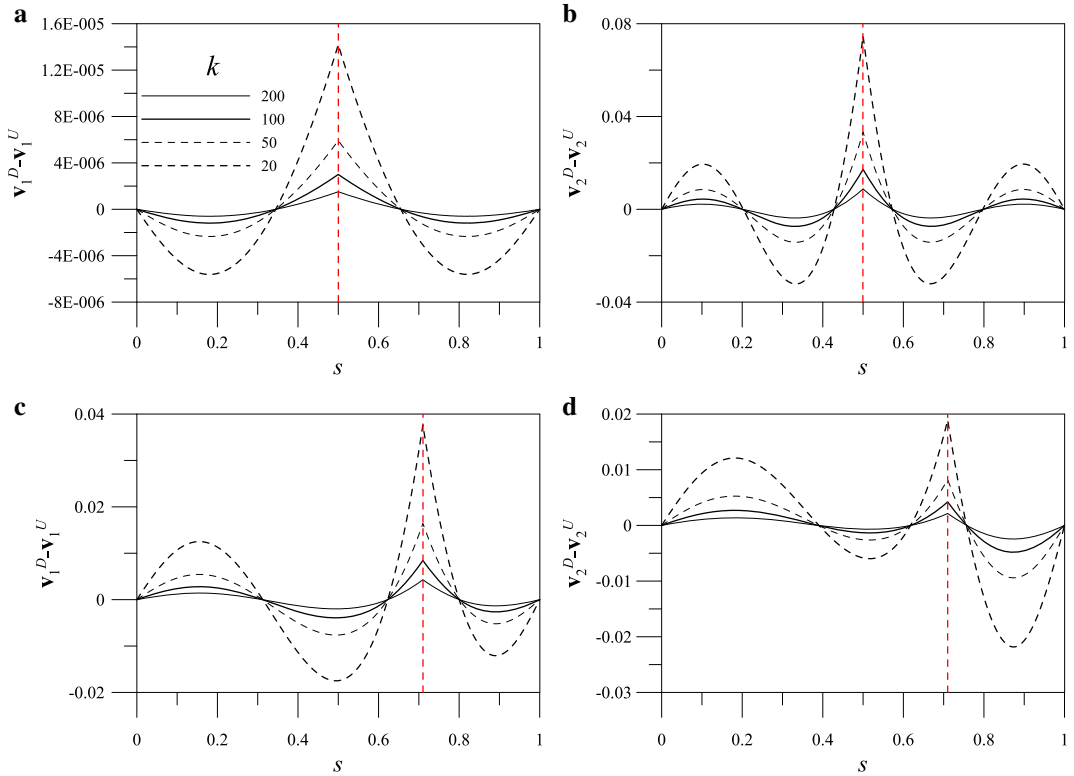

Fig. 5 Change of the first (**a**, **c**) and second (**b**, **d**) transverse modal displacement between the damaged and undamaged states, for different k and damage locations $s = 0.5$ (**a**, **b**) and $s = 0.71$ (**c**, **d**) indicated by *red dashed lines*. (Color figure online)

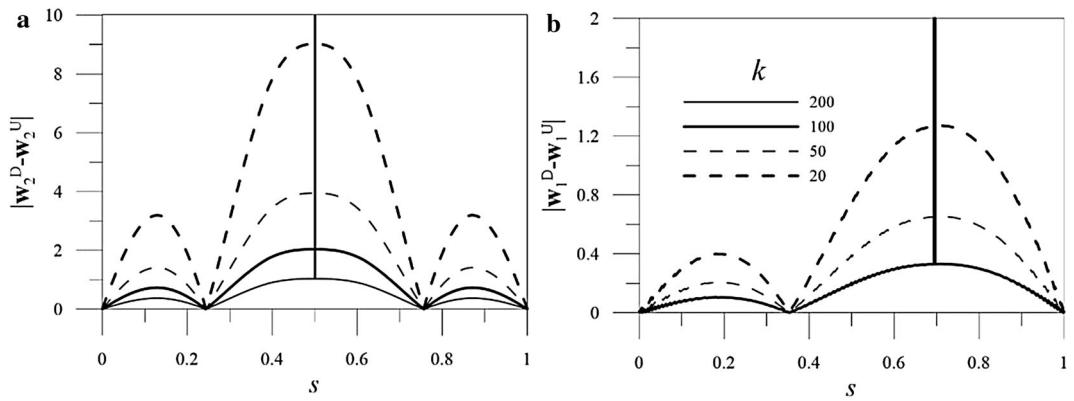

Fig. 6 Change of the first modal curvature for damage located at $s = 0.5$ (**a**) and $s = 0.7$ (**b**)

correspondence of the damage. This result indeed confirms what has been already observed by a number of authors for straight beams [16, 17, 20, 21, 29, 30]. However, for broader damages, the modal curvature difference exhibits significant oscillations outside the damage region and therefore fails to provide a clear indication of the damage position [17, 29]. A much clearer localisation could be obtained by properly filtering the modal curvature difference with the procedure introduced in [17] for Euler–Bernoulli beams. However, when using modal curvature differences for damage detection, one has to face the problem of measuring a highly localised quantity, which in general requires a large number of sensors. Another issue lies in the assessment of the damage intensity that can not be easily related to the modal curvature difference (see, for instance [31]). For this reason, modal curvatures are herein used only for the localization and this additional information is considered in the inverse problem together with the other modal quantities.

4 Inverse problem

The solution of the inverse problem is based on the comparison between the response in the undamaged and damaged states. An optimal estimate of the parameters k and s is obtained by minimizing an objective function which is built as the sum of differences between selected response quantities. In this section, the response quantities obtained by numerically solving the direct problem for assigned values of the damage parameters k and s are assumed as pseudo-experimental data to investigate the accuracy of the optimization procedure in noise-free problems. The same algorithm will be applied to the experimental data in the next section.

As a first step, we consider an objective function which depends only on the first M frequency differences, i.e.,

$$G_f(k,s) = \sum_{i=1}^{M} \left(\frac{\Delta\omega_i(k,s)}{\omega_i^U} - \frac{\Delta\omega_{ei}}{\omega_{ei}^U} \right)^2 \tag{4}$$

which is the sum of the squares of the differences between the numerical $\Delta\omega_i(k,s)$ and experimental $\Delta\omega_{ei}$ frequency variations between the undamaged and the damaged states, normalized with respect to the frequencies of the undamaged arch, ω_i^U and ω_{ei}^U. Equation (4) is a common choice in the literature as frequencies are readily available from the experimental data and require a minimum number of measurement points. Since the $\Delta\omega_i(k,s)$ are not observable in closed-form, they are evaluated at discrete values of k and s, which enables to calculate the function (4) on a grid. The optimal damage parameters $\bar{k}$ and $\bar{s}$ are estimated by successively seeking two distinct minima. First, for each possible damage position s of the grid, the minimum of the function (4) with respect to k is sought. This leads to the following function:

$$\widetilde{G}_f(s) = \min_k G_f(k,s). \tag{5}$$

The solution to the inverse problem is then given by the minimum of $\widetilde{G}_f(s)$ over s.

Let us consider the case of a notch located at $\bar{s} = 0.3$ with $\bar{k} = 20$. The related function $\widetilde{G}_f(s)$ is shown in Fig. 7 extending the summation to two, three and five modes. As inferred from Fig. 4a, if only two frequencies are used, a flat area in the neighborhood of the solution appears in the diagram, as a consequence of the multiple intersections of curves $k_1(s)$ and $k_2(s)$ nearby $s = 0.30$. Although stiffness is correctly identified, location of damage is not. If three frequencies are used, the objective function has its global minimum at the location of damage although some other local minima appear, which are points where $k_i(s)$ curves cross twice. If more than three frequencies are used, a stronger global minimum is attained together with other less pronounced local minima. A drawback of the objective function (5) based on

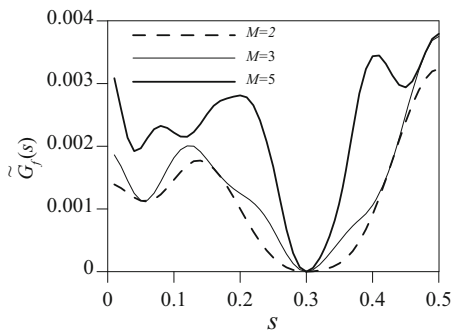

Fig. 7 Objective functions based on the differences between damaged and undamaged frequencies with 2 ($M = 2$, *dashed*), 3 ($M = 3$, *continuous thin*) and 5 modes ($M = 5$, *continuous thick*) for a damage located at $s = 0.3$

frequencies only is that it does not allow distinction between symmetric damage locations. Moreover, in the presence of experimental errors, the global minimum may become less pronounced and in some cases even overtaken by the local minima. For this reason a modified form of the objective function (4) shall be considered to incorporate additional information of a suitable function weighing the modal curvature differences. In this respect, a barrier function $b(s)$ can be added to (4), namely

$$G_{fb}(s,k) = G_f(s,k) + \lambda\, b(s) \tag{6}$$

where λ is a scale factor and $b(s)$ is a convex function which is zero if s falls within the region in which the modal curvature differences localizes the damage and 1 outside this region; solutions that fall outside are penalised in the minimisation process although they are still achievable. A suitable form of the barrier function b is shown in the next section with reference to the experimental data. The introduction of such a regularising term improves the local convexity of the objective function and makes the global minimum stronger; moreover, it removes the indeterminacy due to the symmetry of the structure. In a full-updating procedure, this would make the convergence of the minimization algorithm faster and less prone to experimental errors.

To obtain a more accurate estimate of these two values, an additional term in the objective function is here considered with the idea of weighing also the changes in the modal displacements. It is known from the literature that any objective function based on modal displacement differences has a global minimum at the damage location but also a number of local minima which hence worsen the conditioning of the inverse problem. However, we remark that the presence of the pre-localisation term $b(s)$ partially solves this issue by privileging solutions that fall within the region where the objective function is convex. A suitable term weighing the modal displacement difference is added in the objective function, i.e.,

$$G_{fmb}(k,s) = \sum_{i=1}^{M}\left(\frac{\Delta\omega_i(k,s)}{\omega_i^U} - \frac{\Delta\omega_{ei}}{\omega_{ei}^U}\right)^2 + \sum_{i,j=1}^{N,P}\alpha_j\left(\left|\frac{\Delta v_{i,j}(k,s)}{\bar{v}_{i,j}^U}\right| - \left|\frac{\Delta v_{ei,j}}{\bar{v}_{ei,j}^U}\right|\right)^2 + \lambda\, b(s) \tag{7}$$

where $\Delta v_{i,j}(k,s)$ and $\Delta v_{ei,j}$ are respectively the numerical and experimental changes of the normal components of j-th modal vectors between the undamaged and the damaged states at the i-th measurement point. The constants α_j are suitable weight coefficients. N is the number of modes included in the sum and P is the number of measurement points. In (7) $\bar{v}_{ei,j}^U = \max\{0.1, v_{ei,j}^U\}$ is used to avoid division by a small number, as 0.1 is a threshold comparable to the smallest measured vector component. Note that the number of modes M in the first sum can be different from the number of modes considered in the second sum N weighing the modal displacement difference; this allow the different accurateness in the frequencies and modal displacement estimate to be accounted for. An example of the effects of the modal displacement on the convexity of the objective function is shown in Fig. 8 where the function (5) is compared to (7) with $\lambda = 0$. It is seen that the use of modal shapes in this case eliminates the indeterminacy caused by the symmetry of the structure.

5 Experimental validation

Experiments were carried out by the authors on a prototype double-hinged parabolic arch with mid-span height and length 200 and 1000 mm, respectively [27]. The structure was excited by means of an instrumented hammer and the response read by seven accelerometers equally spaced along the arch and positioned as indicated in Fig. 9. The accelerometers used were mod. PCB-353B04 with a frequency range

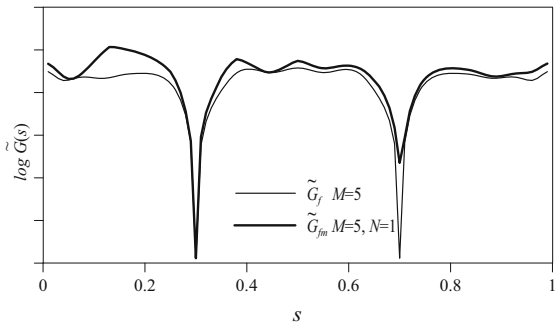

Fig. 8 Objective function obtained comparing the variation of frequencies (5) (*thin*) and the variation of frequencies and the first mode in seven measurement points (7) (with $\lambda = 0$) (*thick*). The actual damage is located at $s = 0.3$

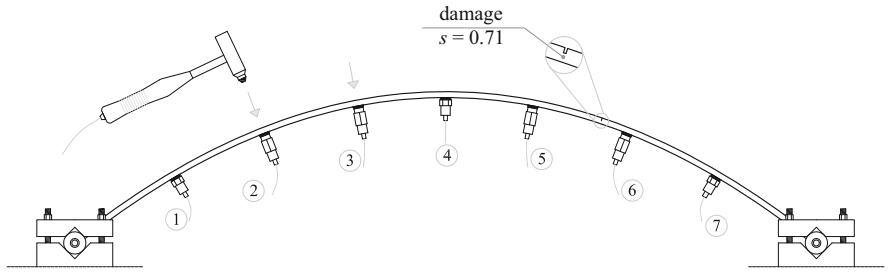

Fig. 9 Schematic representation of the prototype pinned parabolic arch used for the experiments with length 1000 mm and mid-span height 200 mm instrumented by 7 accelerometers

Table 1 Geometrical and mechanical characteristics of the notches

	$h^U - h^D$ (mm)	$\delta = h^D/h^U$	k
D1	1	0.125	557
D2	2	0.250	200
D3	3	0.375	89
D4	4	0.500	39

of 1–7000 Hz, a dynamic range of ±500 g and a sensitivity of 10 mV/g. Each test was repeated ten times. The results presented in this section are the average values over all the measurements.

The damage consisted of an asymmetric notch at the normalised abscissa $s = 0.71$ measured from the left end-side of the arch; four damage intensities were considered, corresponding to an increasing height of the notch (Table 1). The Frequency Response Function (FRF) for the intact arch at each measurements point when the excitation was applied at the accelerometer #2 is shown in Fig. 10, up to 600 Hz. At each measurement point, five peaks are seen in the FRFs, which correspond to the first five modes; the corresponding eigenfrequencies and eigenmodes have been extracted by means of a multimode method using a nonlinear least-squares approach (see for instance [32]).

Table 2 reports the eigenfrequencies in both undamaged and damaged states and the corresponding variations. The ratio of standard deviation to the mean, is very low, of the order of 1/100 Hz for all repetitions. The modes presenting the highest ratio are those which have a node in the vicinity of the measurement or excitation points. A slight increment of this ratio is observed when damage increases.

The prelocalisation of damage, which is needed to construct the barrier function $b(s)$, can be obtained through the modal curvature difference. In particular, the following function here called *localization index* based on the comparison between the damaged and undamaged modal curvatures has been effectively used in the literature [24, 31]:

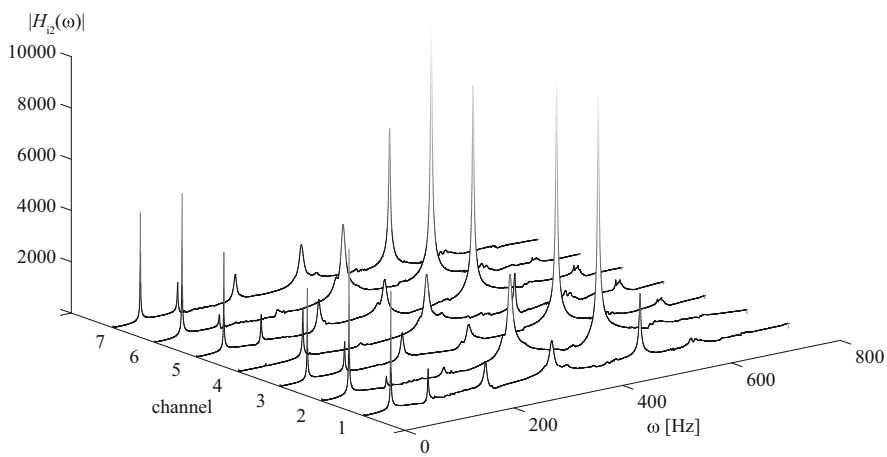

Fig. 10 Frequency response functions of the intact arch for an excitation at accelerometer #2

Table 2 Experimental natural frequencies of the undamaged (U) and damaged (D) arch (Hz) and corresponding variations

	ω_{e1}	$\frac{\lvert\Delta\omega_{e1}\rvert}{\omega_{e1}^U}$ (%)	ω_{e2}	$\frac{\lvert\Delta\omega_{e2}\rvert}{\omega_{e2}^U}$ (%)	ω_{e3}	$\frac{\lvert\Delta\omega_{e3}\rvert}{\omega_{e3}^U}$ (%)	ω_{e4}	$\frac{\lvert\Delta\omega_{e4}\rvert}{\omega_{e4}^U}$ (%)	ω_{e5}	$\frac{\lvert\Delta\omega_{e5}\rvert}{\omega_{e5}^U}$ (%)
U	50.40		118.94		224.80		346.33		508.55	
D1	50.34	0.12	118.92	0.02	224.63	0.08	346.08	0.07	508.28	0.05
D2	50.18	0.44	118.92	0.02	224.62	0.08	345.02	0.38	507.89	0.13
D3	49.91	0.97	118.91	0.03	223.96	0.37	343.20	0.90	507.05	0.29
D4	49.23	2.32	118.91	0.03	222.05	1.22	339.48	1.98	505.18	0.66

$$LI_i = \left\{ \sum_{m=1}^{M} \left[(w_{m,i}^U)^2 - (w_{m,i}^D)^2 \right] \right\}^2, \tag{8}$$

where $w_{m,i}^U$ and $w_{m,i}^D$ are the m-th modal curvatures at nodes i in the undamaged and damaged states, respectively. To provide an accurate estimate of the curvature, the modal displacements have been interpolated by a cubic spline. The corresponding index (8) calculated with the first three modes in the four damage scenarios is shown in Fig. 11 together with the corresponding barrier function. For all damage intensities, the damage region estimated by *LI* contains the actual damage location represented by a red dashed line in the figure which confirms the validity of the method. The barrier function $b(s)$ is chosen to be a tapered cosine function with expression

$$b(s) = \begin{cases} 0 & -\frac{1}{2} \le s - s_0 \le \frac{1}{2} \;\&\; \alpha + 2(s - s_0) \ge 0 \\ & \;\&\; \alpha - 2(s - s_0) \ge 0 \\ \frac{1}{16}\left(1 + \sin(\frac{\pi}{\alpha}(s - s_0))\right)^4 & \frac{1}{2} \;\&\; \alpha + 2(s - s_0) < 0 \\ \frac{1}{16}\left(1 - \sin(\frac{\pi}{\alpha}(s - s_0))\right)^4 & \frac{1}{2} \;\&\; \alpha + 2(s - s_0) \ge 0 \;\&\; \alpha - 2(s - s_0) < 0 \\ 1 & |s - s_0| > \frac{1}{2} \end{cases} \tag{9}$$

where s_0 is the center of the damaged region and α determines its width.

The results of the identification problem carried out by minimising the function (6) based on the eigenfrequency variations are reported in Table 3 for all the damage configurations examined in terms of damage position s and intensity k or alternatively in terms of the relative stiffness variation and damage height (see Eq. (3)). The results of the problem show that estimate of the damage intensity and position are achieved with different accuracies. On the one hand in fact, damage is located in a remarkably accurate manner for damage cases D1, D3 and D4 whereas a small error occurs for D2 (below 1.5 %). On the other hand, the equivalent spring stiffness is overestimated in all cases but D4 (−5.00 %); the error monotonically decreases up to 6.59 % for D3 and not surprisingly, the largest errors regard the weakest damage D1. This low accuracy in determining the damage intensity with the solely use of frequency variations has been already pointed out in the literature (see, e.g. [27]). To overcome this limitation the additional information coming from the mode shape variations could be used in the objective function.

The first two experimental mode displacement differences are shown in Fig. 12a, b together with the corresponding modal curvature differences (c and d).

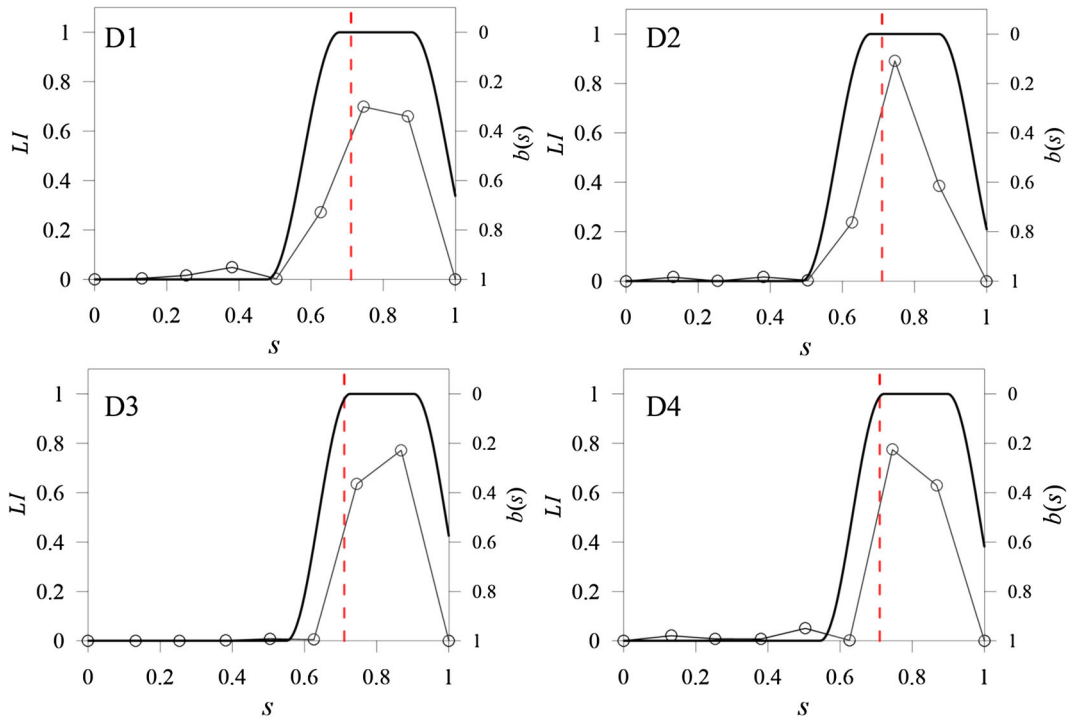

Fig. 11 Localization index calculated through (8) by using the first three modes (*grey circled line*). The *black line* shows the corresponding barrier function defined in (9) whereas the actual damage position is indicated by a *red dashed line*. (Color figure online)

Table 3 Damage parameters identified by considering the first five eigenfrequency variations in the objective function (6) and (7) for the four damage cases examined

	G_{fb}				G_{fmb}			
	k	e_k (%)	s	e_s (%)	k	e_k (%)	s	e_s (%)
D1	648	16.3	0.71	0.0	542	−2.69	0.72	1.4
D2	237	18.5	0.72	1.4	197	−1.50	0.72	1.4
D3	97	8.99	0.71	0.0	90	1.10	0.72	1.4
D4	38	−2.50	0.71	0.0	38	−2.50	0.71	0.0

The relative errors are computed with respect to the model value in Table 1

It is seen from the figure that multiple peaks appear in the difference when considering modal displacements, whereas a more localised information can be extracted from the modal curvature difference. In the case of mode shapes, these peaks, whose intensity monotonically increases with the damage intensity, are located in a region close to, but not correspondent, with the actual damage position (represented by a dashed red line). As already pointed out, such a circumstance makes the solely use of eigenmode difference in the damage localization problematic and potentially leading to false indications. However, their use in the objective function together with the eigenfrequencies variation can lead to a more accurate evaluation of the damage parameters.

In this respect, in Fig. 13 the objective function (7), built by considering the first five eigenfrequencies and only the first mode shape, is shown for damage configurations D1 and D4. Adding the modal components enables one to obtain a well defined unique minimum, although several other local minima can

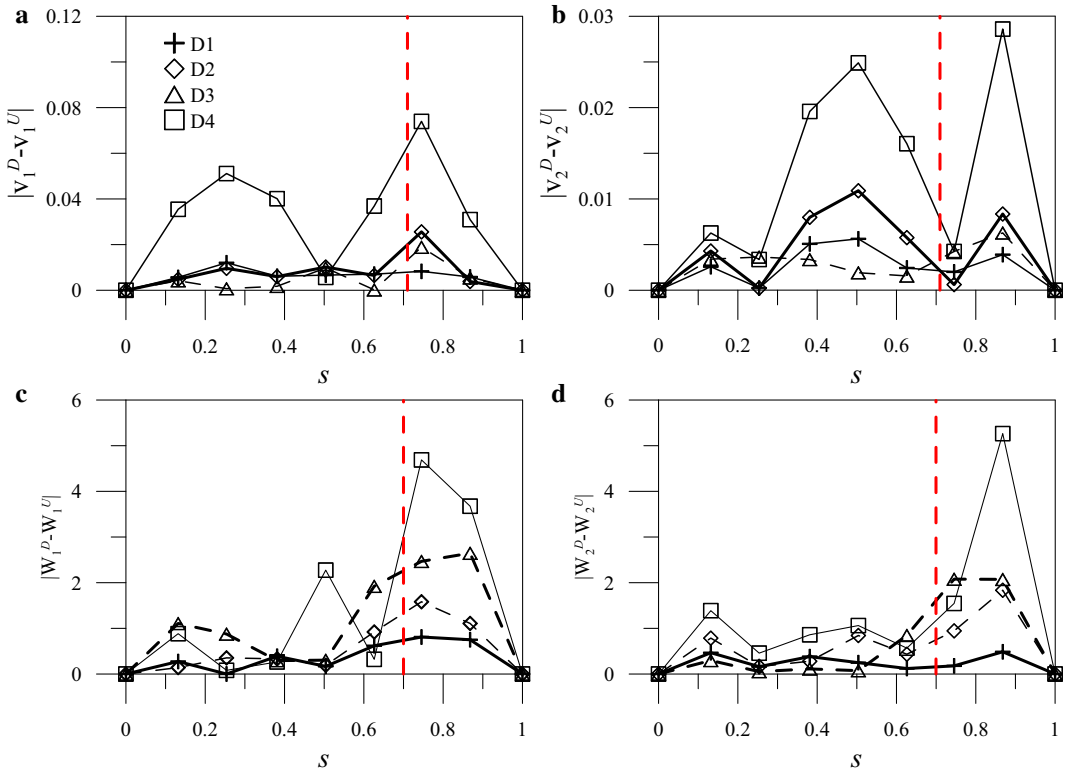

Fig. 12 First **a** and second **b** experimental modal displacement difference between the damaged and undamaged system for the four damage scenarios considered. First **c**, and second **d** experimental modal curvature differences. (Color figure online)

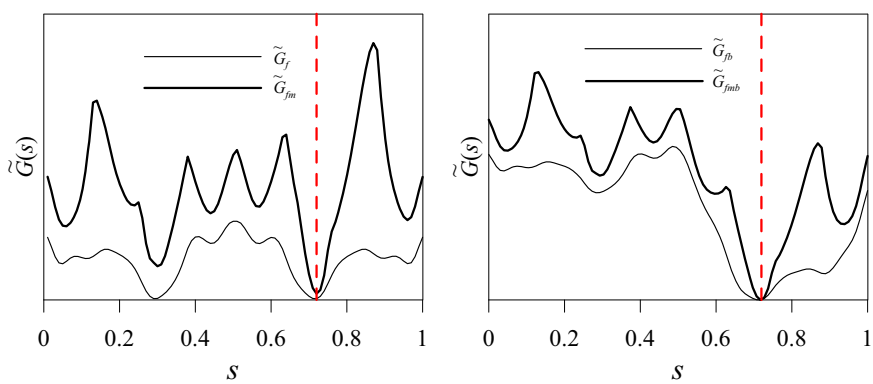

Fig. 13 Objective functions obtained for D1 and D4 considering the variation of frequencies (*thin*) and the variation of the first mode in seven measurement points (*thick*). (Color figure online)

still be observed. Table 3 summarises the identification results in terms of damage position and equivalent spring stiffness. For all damage cases, the intensity is underestimated (except for D3), but the corresponding overall error decreases. Here also, the largest errors regard the weakest damage D1, for which the error on the stiffness greatly decreases with respect to the case with five frequencies: the equivalent stiffness was estimated with an error of 16.3 % that by means of the new functional has been reduced to −2.69 %. A similar trend is seen for all damage scenarios but the more severe one D4 for which the position is still accurately identified ($e_s = 0.0\,\%$), yet the addition of the modal shape does not contribute to an improved intensity estimate. The damage position is identified with a mean error of 1.4 % which is larger than the

case of the objective function solely based on the frequency variations. In this case, the second close minimum provides better stiffness and notch depth but its position slightly moves towards the right pinned end of the arch.

6 Conclusions

The identification of position and severity of damage based on the observation of dynamic response quantities is an inverse problem, which presents different sources of indeterminacy and ill conditioning. In this paper we have investigated the role of natural frequencies, mode shapes and curvatures in providing a unique solution using a two-parameter objective function that minimizes the difference between numerical and experimental response quantities. The system under investigation is a double-hinged parabolic arch with localised damage of a notch type. Different damage intensities have been considered.

Differently from simply supported straight beams, if only the change of natural frequencies is considered, at least the first three frequencies are needed to uniquely determine the two damage parameters k and s, for the considered arch. One of the major sources of indeterminacy is due to the fact that the change of natural frequencies is not sufficient to discern between symmetric damage locations. This can be removed by adding to the objective function the change of modal components or the change of modal curvatures. In this regard, it has been shown that the change of modal curvatures between the undamaged and damaged states is extremely localized and very difficult to be used for the estimate of damage parameters. Nevertheless, it can be used to build a penalty function which enhances the contribution of selected parts of the objective function, in particular those nearby the locations where the change of curvature is larger. The penalty function not only does indicate which half of the structure is damaged, but also helps in improving the convexity of the objective function, limiting its oscillations and the related local minima that, in the presence of experimental errors, can lead to an incorrect estimate. The increased robustness of the estimate has been assessed based on experimental investigations on the arch under study, showing satisfactory effectiveness of the procedure described, apart from the case of very weak damage. The study also shows that discrepancies between the model and the real structure have an influence on the parameter estimates, and therefore both the quality of the experimental data and an accurate modelling are fundamental if reliable results are to be obtained.

References

1. Farrar CR, Lieven NJ (2007) Damage prognosis: the future of structural health monitoring. Philos Trans R Soc A 365:623–632
2. Fan YF, Zhou J, Hu ZQ, Zhu T (2007) Study on mechanical response of an old reinforced concrete arch bridge. Struct Control Health Monit 14(6):876–894
3. Jiang S, Xu F, Fu C (2010) Intelligent damage identification model of an arch bridge based on box-counting dimension and probabilistic neural network. J Comput Inf Syst 6(4):1185–1192
4. Magalhães F, Cunha A, Caetano E (2012) Vibration based structural health monitoring of an arch bridge: from automated OMA to damage detection. Mech Syst Signal Process 28:212–228
5. Benedettini F, Capecchi D (1988) A perturbation technique in sensitivity analysis of elastic structures. Meccanica 23(1):5–10
6. Vestroni F, Capecchi D (2000) Damage detection in beam structures based on frequency measurements. J Eng Mech 126(7):761–768
7. Montalvao D (2006) A Review of vibration-based structural health monitoring with special emphasis on composite materials. Shock Vib Dig 38(4):295–324
8. Papadimitriou C, Ntotsios E, Giagopoulos D, Natsiavas S (2012) Variability of updated finite element models and their predictions consistent with vibration measurements. Struct Control Health Monit 19(5):630–654
9. Nguyen VV, Dackermann U, Li J, Alamdari MM, Mustapha S, Runcie P, Ye L (2015) Damage identification of a concrete arch beam based on frequency response functions and artificial neural networks. Electron J Struct Eng 14(1):75–84
10. Vestroni F, Pau A (2011) Dynamic characterization and damage identification in dynamic inverse problems: theory and application. In: Gladwell GMR, Morassi A (eds) CISM Courses and Lectures, n. 529, pp 151–178
11. Cerri MN, Vestroni F (2003) Identification of damage due to open cracks by changes of measured frequencies. In: Proceedings of XVI AIMETA congress of theoretical and applied mechanics, Ferrara
12. Kim J-T, Ryu Y, Cho H, Stubbs N (2003) Damage identification in beam-type structures: frequency-based method vs mode-shape-based method. Eng Struct 25(1):57–67
13. Greco A, Pau A (2012) Damage identification in Euler frames. Comput Struct 92–93:328–336
14. Cerri MN, Ruta GC (2004) Detection of localised damage in plane circular arches by frequency data. J Sound Vib 270(1–2):39–59

15. Cerri MN, Dilena M, Ruta GC (2008) Vibration and damage detection in undamaged and cracked circular arches: experimental and analytical results. J Sound Vib 314(1–2): 83–94
16. Dessi D, Camerlengo G (2015) Damage identification techniques via modal curvature analysis: overview and comparison. Mech Syst Signal Process 52–53:181–205
17. Ciambella J, Vestroni F (2015) The use of modal curvatures for damage localization in beam-type structures. J Sound Vib 340:126–137
18. Pandey AK, Biswas M, Samman MM (1991) Damage detection from changes in curvature mode shapes. J Sound Vib 145(2):321–332
19. Ciambella J, Vestroni F, Vidoli S (2011) Damage observability, localization and assessment based on eigenfrequencies and eigenvectors curvatures. Smart Struct Syst 8(2):191–204
20. Chandrashekhar M, Ganguli R (2009) Damage assessment of structures with uncertainty by using mode-shape curvatures and fuzzy logic. J Sound Vib 326(3–5):939–957
21. Cao M, Radzieński M, Xu W, Ostachowicz W (2014) Identification of multiple damage in beams based on robust curvature mode shapes. Mech Syst Signal Process 46(2): 468–480
22. Dilena M, Morassi A (2011) Dynamic testing of a damaged bridge. Mech Syst Signal Process 25(5):1485–1507
23. He S, Rose LRF, Wang CH (2013) A numerical study to quantify delamination damage of composite structures using inverse the method. Aust J MultiDiscip Eng 10(2): 145–153
24. Quaranta G, Carboni B, Lacarbonara W (2016) Damage detection by modal curvatures: numerical issues. J Vib Control 22(7):1913–1927 (first published online 2014)
25. Cao M, Xu W, Ostachowicz W, Su Z (2014) Damage identification for beams in noisy conditions based on Teager energy operator-wavelet transform modal curvature. J Sound Vib 333(6):1543–1553
26. Cao M, Qiao P (2009) Novel Laplacian scheme and multiresolution modal curvatures for structural damage identification. Mech Syst Signal Process 23(4):1223–1242
27. Pau A, Greco A, Vestroni F (2011) Numerical and experimental detection of concentrated damage in a parabolic arch by measured frequency variations. J Vib Control 17(4):605–614
28. Chidamparam P, Leissa AW (1993) Vibrations of planar curved beams, rings and arches. Appl Mech Rev 46(9): 467–483
29. Lestari W, Qiao P, Hanagud S (2007) Curvature mode shape-based damage assessment of carbon/epoxy composite beams. J Intell Mater Syst Struct 18(3):189–208
30. Unger JF, Teughels A, De Roeck G (2006) System identification and damage detection of a prestressed concrete beam. J Struct Eng 132(11):1691
31. Abdel Wahab M, De Roeck G (1999) Damage detection in bridges using modal curvatures: application to a real damage scenario. J Sound Vib 226(2):217–235
32. Ewins DJ (2000) Modal testing, theory, practice, and application, 2nd edn. Research Studies Press, Baldock